An adiabatic model for the photodissociation of CH_3SH in the first ultraviolet absorption band

Jonathan E. Stevens, Hyo Weon Jang, Laurie J. Butler, and John C. Light
Department of Chemistry and The James Franck Institute, The University of Chicago, Chicago, Illinois 60637

(Received 19 December 1994; accepted 31 January 1995)

The photodissociation of CH_3SH in the first absorption band is studied via *ab initio* computation of the relevant potential energy surfaces and exact quantum scattering calculations. The effective valence shell Hamiltonian (H^{ν}) *ab initio* many-body perturbation technique is used to calculate the global ground $X\ ^1A'$ and $1\ ^1A''$ surfaces as functions of the C–S and S–H internuclear distances. The finite range scattering wave function (FRSW) time-independent quantum scattering method is used to compute the adiabatic dynamics of S–H and C–S bond fission on the $1\ ^1A''$ surface following excitation. Two calculations are performed, one in which the ground state is represented by a cubic spline function fitted to the *ab initio* data and another in which it is represented as the sum of two uncoupled Morse oscillators. Absorption spectra as well as the branching ratios and photofragment translational energy distributions corresponding to various excitation energies are presented and compared to recent experimental results. A final calculation examines how the branching ratio and product vibrational state distribution changes for the photodissociation of a CH_3SH molecule with one quantum of vibrational excitation in the C–S stretch. © *1995 American Institute of Physics.*

I. INTRODUCTION

The photoexcitation and subsequent dissociation of methyl mercaptan (CH_3SH) in the first and second absorption bands has been the subject of extensive experimental[1–10] and theoretical[11–15] study. Two channels of photodissociation are experimentally observed. Fission of the S–H bond is the predominant process, but a small amount of C–S bond fission is also observed, increasing in proportion to S–H bond fission with increasing excitation energy.[3,7,16]

Recent experiments by Butler and co-workers[6,7] employing crossed laser–molecular beam studies and emission experiments have probed the dynamics of the competing channels in CH_3SH. The highly anisotropic photofragment angular distributions measured in the crossed laser–molecular beam experiments show that both C–S and S–H fission processes occur on a subpicosecond time scale upon excitation in both the lower and upper absorption bands, despite the fact that excitation in the higher energy absorption band is to a surface that is adiabatically bound in both bond fission coordinates. The measured kinetic energy distributions show that most of the energy available from excitation goes into the relative kinetic energy of the photofragments, leaving the SH and CH_3S photoproducts relatively vibrationally cold. The emission spectroscopy studies show emission into one excited quanta of the S–H stretch vibrational mode following excitation in the first absorption band, and emission into a progression of C–S stretching vibrational states following excitation in the second absorption band.

Electronic structure calculations of CH_3SH[11–15] indicate that the states accessed by irradiation in the first and second absorption band are the $1\ ^1A''$ and $2\ ^1A''$ states, respectively. These calculations suggest that the $1\ ^1A''$ state is of mixed Rydberg–valence character, primarily valence. The $2\ ^1A''$ state is primarily Rydberg in character, although calculations[11–14] suggest it has some valence character and emission spectroscopy[7] indicates that there is $n \rightarrow \sigma^*$ (C–S) antibonding character in the Franck–Condon region at 193 nm. Constructing simple adiabatic correlation diagrams suggests that the $2\ ^1A''$ is bound in both the C–S and S–H internuclear distance coordinates while the lower $1\ ^1A''$ surface is dissociative in both coordinates. This expectation is corroborated, at least in the coordinate of the S–H internuclear distance, by the *ab initio* calculations of the excited potential surfaces of Mouflih *et al.*[12,13] Further confirmation is provided by computations of the relevant surfaces performed in collaboration with Butler *et al.*'s experimental study, using the *ab initio* effective valence shell Hamiltonian method of Freed and co-workers.[7,14] These calculations extend over the coordinates of both the S–H and C–S internuclear distances. Similar cuts of these surfaces have also been computed by Yarkony and co-workers using configuration interaction techniques.[15]

Butler and co-workers infer that molecular dissociation in the second absorption band must arise from strong nonadiabatic coupling of the $2\ ^1A''$ and $1\ ^1A''$ surfaces, while dissociation following irradiation in the first absorption band may be understood primarily in terms of evolution of the molecular system upon the single Born–Oppenheimer $1\ ^1A''$ surface. In particular, the preferential fission of the S–H over the C–S bond may be understood by considering the shape of the $1\ ^1A''$ potential surface in the Franck–Condon region, where it is repulsive in the S–H internuclear coordinate but has a small exit channel barrier along the coordinate of the C–S internuclear distance. This small barrier results from an avoided crossing of the $1\ ^1A''$ and $2\ ^1A''$ surfaces, and inhib-

its C–S bond fission by making the Franck–Condon region of the $1\ ^1A''$ surface weakly bonding. Although sufficiently high excitation energies in the first absorption band provide the molecular system with sufficient energy to surmount this barrier, the forces in the Franck–Condon region still drive the molecule toward S–H bond fission and not toward S–C bond fission.

Although dissociation upon excitation in the second absorption band requires including electronically nonadiabatic transitions, we seek here to investigate the importance of nonadiabatic effects upon dissociation in the first absorption band, where one might postulate that hops to the upper, bound state might influence the branching between competing bond fission channels.[17] The photodissociation process may be thought of here as a molecular ''half-collision'' in which electronic excitation to the $1\ ^1A''$ surface promotes the molecule to the transition state region of a reaction pathway leading from CH_3 and SH reactants to CH_3S and H products. One might postulate that nonadiabatic dynamics plays a role in the motion of the system along this reaction pathway in the transition state region, where an upper, bound surface (in this case the $2\ ^1A''$ surface) lies energetically proximate to the surface of the reaction pathway and nonadiabatic hops from the lower electronic state to the upper bound state might occur. This work presents a purely adiabatic model of the photodissociation of CH_3SH in the first absorption band to see if one can obtain reasonable agreement with experimental data if one ignores any influence of nonadiabatic effects on the dynamics on the lower reactive $1\ ^1A''$ potential surface. The experimentally determined absorption spectrum will be compared to absorption spectra obtained from the calculations. Other theoretically predicted results, in particular the branching ratios and translational/internal vibrational energy distributions of the fragments, will be compared to the outcome of the experiments of Butler *et al.* Comparison is also made to recent experimental studies in Wittig's[8] and Dixon's[9] laboratories which determine fragment translational/vibrational distributions corresponding to S–H fission following $X\ ^1A' \rightarrow 1\ ^1A''$ excitation. We use a two-dimensional Born–Oppenheimer potential energy surface calculated for the excited ($1\ ^1A''$) state in conjunction with two different ground state surfaces, one fit to *ab initio* data points and another constructed semiempirically. The *ab initio* calculations of the surfaces use the effective valence shell Hamiltonian (H^ν) of Freed and co-workers and vary only the C–S and S–H bond distances while holding the C–S–H bending angle and the geometry of the methyl group fixed. Time-independent exact quantum mechanical dynamics calculations were performed on the surfaces using the finite range scattering wave function (FRSW) method. This method has been successfully applied to several model and real scattering and resonance problems.[18,19] Section II discusses the computation of the potential energy surfaces. Section III discusses the definition of the Hamiltonian operator for the dynamical calculations, details the construction of contracted basis functions from the primitive ones, and explains the construction of the Hamiltonian matrix. Section IV discusses the behavior of the asymptotic scattering wave function. Section V details the system of linear equations used to solve for the outgoing scattering wave functions. Section VI presents the calculated absorption spectra and product channel branching, as well as internal vibrational energy distributions of products at several wavelengths. We analyze the results with respect to the available experimental data and with respect to the qualitative features of the dynamics revealed. This section also presents the computed results for uv photodissociation of a CH_3SH molecule with one quantum of vibrational excitation in the C–S stretch.

II. POTENTIAL ENERGY SURFACES

The two-dimensional global potential energy surfaces for the ground ($X\ ^1A''$) and excited ($1\ ^1A''$) surfaces of methyl mercaptan were computed using the effective valence shell Hamiltonian (H^ν) method of Freed and co-workers, a size extensive, fully correlated multireference perturbative *ab initio* scheme. A complete description of this method is available elsewhere,[20] and the high accuracy of this method has been demonstrated in recent calculations.[21] The CH_3SH global potential surface computations mark the first use of this method to calculate global potential surfaces for a highly nontrivial system using a restricted valence space. They are also unique in demonstrating that many-body theory methods are capable of computing global potential surfaces. Reference 14 describes details of the choice of a suitable valence space for this system usable over wide ranges of nuclear geometries, as well as a full detailing of the H^ν calculations. An abbreviated description of the computations is provided here.

The H^ν calculations employ a 4–31G** basis set with the addition of diffuse (exponent=0.02 a.u.$^{-2}$) s and p functions on carbon and sulfur, for a basis of 62 Gaussian-type orbitals with 44 symmetry-adapted a' orbitals and 18 a'' orbitals.[22] The equilibrium geometry in the degrees of freedom that are held fixed in the scattering calculations is taken from the previous STO-3G optimization of Dill and McLafferty.[23] Dill and McLafferty's geometry deviates from the experimental geometry;[24] most notably, the C–S equilibrium bond length is underestimated by 0.039 a.u. Trial calculations show that the third order H^ν energies and vertical excitations differ by an average of only 0.05 eV between the two geometries. As noted, the *ab initio* surface calculations hold the C–S–H angle and the geometry of the methyl group fixed, varying only the C–S and S–H internuclear distances.

The valence space for the H^ν calculations is defined by the two highest occupied orbitals in the SCF ground state, $10a'$ and $3a''$, and the three lowest-lying excited orbitals, $11a'$, $12a'$, and $13a'$. The ground state occupied valence orbitals are canonical RHF orbitals, while the remaining orbitals in the valence space are optimized independently from SCF calculations for low-lying excited states to produce improved virtuals orbitals (IVO's). In the region near the ground state equilibrium geometry, the excitation to the $1\ ^1A''$ surface may be described in zeroth order as a $3a'' \rightarrow 11a'$ excitation.

The third order H^ν computation simultaneously generates the $X\ ^1A'$ and $1\ ^1A''$ surfaces. A contour plot of the $1\ ^1A''$ surface is shown in Fig. 1. The data has been fit using the two-dimensional spline method employed by Weide

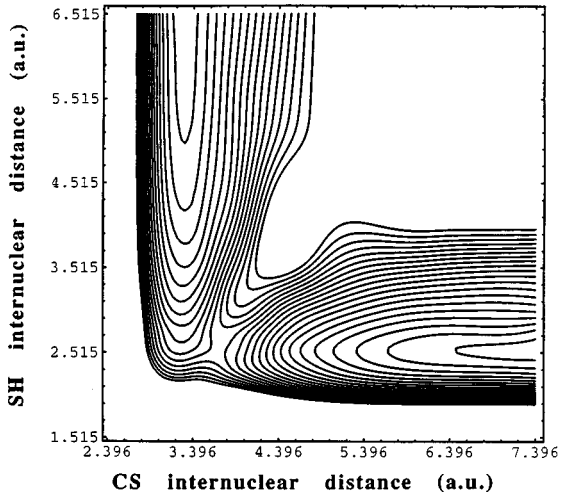

FIG. 1. Contour plot of the 1 $^1A''$ surface along the C–S and S–H bond coordinates as constructed from a two-dimensional cubic spline fit to the third order H^ν *ab initio* data points. The separation between contours is 0.0071 hartree.

et al.[25] to fit the S_1 excited surface of CH_3OH for time-dependent studies of the photodissociation of that system. Figure 2 shows contour plots of the two choices for the ground state surface of CH_3SH. The one in the upper frame is simply the sum of two independent Morse oscillators with frequencies corresponding to the S–H and C–S vibrational frequencies.[26] The one in the lower frame is a two-dimensional spline fit to the *ab initio* data. We employ each of these ground state surfaces in turn to model the photodissociation. The two ground state surfaces differ primarily in the location of the minimum in the potential well; the surface defined as the sum of Morse oscillators defines the minimum to be located at the equilibrium bond lengths determined by Dill and McLafferty (located at a CS internuclear distance 0.039 a.u. less than experimentally determined), while the minimum for the spline-fitted surface is located at slightly shorter C–S bond distances (approximately 0.029 a.u. less than the equilibrium distance as determined by the H^ν calculations). Our calculations, using these two choices for the ground state surface, thus investigate the effect that the positioning of the ground state minimum along the C–S internuclear distance has upon the dissociation dynamics.

III. HAMILTONIAN AND BASIS

The theoretical model for the photodissociation of CH_3SH uses an exact time-independent quantum mechanical method to calculate the Franck–Condon intensity $|\langle\chi_i|\Psi_f^-\rangle|^2$ for the initial bound state on the ground state potential energy surface and the final dissociative state on the first excited one as a function of photon energy. The total angular momentum is taken to be zero ($J=0$). In addition, the CH_3 group is modeled as a pseudoatom and the bond angle of H–S–C is fixed at the equilibrium value of 95.1 deg. This simplification reduces the problem to one of two degrees of freedom, the S–H and C–S internuclear distances.

A suitable coordinate system to represent the dynamics is that of the S–H and S–C bond coordinates. This system is

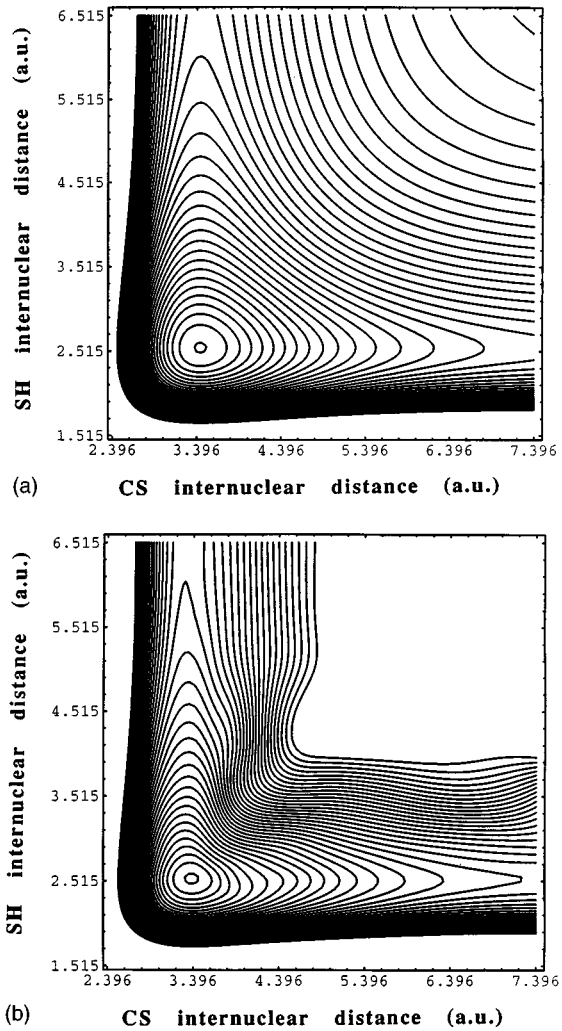

FIG. 2. Contour plots of the ground state $X\ ^1A'$ state along the C–S and S–H bond coordinates. The upper plot is of the semiempirical surface constructed as the sum of two independent Morse oscillators. The lower plot is of the surface obtained from a two-dimensional spline fit to the *ab initio* data points. The separation between contours is 0.0071 hartree.

appropriate for the present problem as it allows the bending angle to be fixed. The total angular momentum is explicitly conserved even with the fixed bond angle. These are features which are not shared by the widely used Jacobi coordinate system. These bond coordinates were successfully applied to the methanol photodissociation by Marston *et al.* who calculated the Franck–Condon intensity by the time dependent wave packet propagation method.[25] The only inconvenient feature is that the powerful successive diagonalization-truncation[27] scheme cannot be implemented straightforwardly since the two variables are fully mixed in the Hamiltonian operator in this coordinate system. As a result, the size of the matrix subject to diagonalization is rather larger than it would be in the successive diagonalization-truncation scheme.

For the total angular momentum zero ($J=0$), the Hamiltonian operator in the bond coordinate system is given by

$$\hat{H}(q_1,q_2)=\frac{-1}{2}\sum_{\alpha,\beta=1}^{2}\frac{\partial}{\partial q_\alpha}\mathbf{G}_{\alpha\beta}\frac{\partial}{\partial q_\beta}+V(q_1+q_2), \tag{1}$$

$$\mathbf{G}=\begin{bmatrix}\frac{1}{\mu_{AB}}-\frac{\xi^2 q_1^2}{m_A^2\Gamma} & \frac{1}{m_A}\left(\nu-\frac{\xi^2 q_1 q_2}{m_A\Gamma}\right)\\ \frac{1}{m_A}\left(\nu-\frac{\xi^2 q_1 q_2}{m_A\Gamma}\right) & \frac{1}{\mu_{AC}}-\frac{\xi^2 q_2^2}{m_A^2\Gamma}\end{bmatrix},$$

$$\frac{1}{\mu_{AB}}=\frac{1}{m_A}+\frac{1}{m_B},\qquad \frac{1}{\mu_{AC}}=\frac{1}{m_A}+\frac{1}{m_C},$$

$$\Gamma=\frac{1}{\mu_{AC}}q_1^2+\frac{1}{\mu_{AB}}q_2^2-2\frac{1}{m_A}\nu q_1 q_2,$$

$$\nu=\cos\,\theta,\qquad \xi=\sin\,\theta,$$

where A, B, and C stand for S, H, and CH_3, respectively. The q_1, q_2 are the bond lengths of S–H and of S–C, respectively, and θ is the fixed bond angle between the two bonds. The m_X stands for the mass of X. The potential energy, $V(q_1,q_2)$, reduces to two different asymptotic forms depending on the arrangement channel,

$$\begin{aligned}&V(q_1,q_2)\rightarrow U_1(q_1)\ \text{ as }\ q_2\rightarrow\infty,\\ &\text{or }\ U_2(q_2)\ \text{ as }\ q_1\rightarrow\infty.\end{aligned} \tag{2}$$

This is the representation of the Hamiltonian operator applied to CH_3OH photodissociation by Marston *et al.*[25]

The potential may correspond to the ground or the first excited state. For the ground state Hamiltonian, we focus on the bound states χ_i which may be expanded by basis functions satisfying zero boundary conditions. For the excited one, the scattering wave functions are expanded by the same basis functions plus energy independent auxiliary functions in the FRSW method.[18] In particular, we use the unit normalized form of the interior Labatto shape functions $\{u_i(q_\alpha)\}_1^{N_\alpha}$ as the primitive basis functions.[28] The more efficient contracted basis set may be composed of the direct product functions of each one-dimensional contracted basis functions of q_1 and q_2 motions. For the excited state, each one-dimensional contracted function may be selected by considering the expectation that each one-dimensional motion will become either vibrational or dissociative depending on the particular arrangement channel asymptotically. For example, the basis for q_1 motion is obtained by combining two sets of eigenfunctions of $\hat{H}(q_1,q_2)$ determined at two values of q_2. One set of functions is obtained by diagonalizing $\hat{H}(q_1,q_2)$ for q_2 fixed at the outer boundary of the q_2 functions. These are eigenfunctions corresponding to q_1 vibrational motion. The other set is obtained for q_2 fixed at the minimum of $V(q_1,q_2)$ as q_1 approaches its asymptotic region. These functions are translational (dissociative) functions for q_1. Then, when we orthonormalize the combined set through canonical orthonormalization transformation, the duplicate functions are discarded. The resulting orthonormalized functions serve as the one-dimensional basis functions for the q_1 motion. A parallel procedure produces the one-dimensional basis functions for the q_2 motion. The final two-dimensional basis set is obtained by taking the direct product of the two contracted one-dimensional basis functions.

Numerical calculations show that the basis set determined as described above is not suitable to give sufficiently converged results. A refinement can be made by adding more primitive basis functions to the set of one-dimensional eigenfunctions. Since we evaluate the wave functions in the asymptotic region, it is reasonable to add functions one by one toward inside from the outer boundary until no more linearly independent functions are produced by the canonical orthonormalization transformation. This procedure produces a "saturated" one-dimensional contracted basis set, and it gives converged results.

A similar contracted one-dimensional basis set can be constructed for the ground state. In this case, however, the contracted functions are obtained as only one set of one-dimensional eigenfunctions of $\hat{H}(q_1,q_2)$ along the minimum potential energy cut, which functions may correspond to one-dimensional vibrational motion for each degree of freedom.

The Hamiltonian matrix in the contracted two-dimensional basis set is diagonalized to produce discrete eigenfunctions and eigenvalues for both the ground and the first excited electronic state. The eigenfunctions serve as the initial bound state χ_i and as part of the expansion functions for the scattering wave function Ψ_f^-.

The various terms of the Hamiltonian matrix in the primitive basis set $\{u_i(q_1)\}_1^{N_1}\otimes\{u_j(q_2)\}_1^{N_2}$ are given, with Gaussian–Lobatto quadrature approximations, by

$$\begin{aligned}&\left\langle u_i(q_1)u_j(q_2)\left|\frac{\partial}{\partial q_1}\mathbf{G}_{12}\frac{\partial}{\partial q_2}\right|u_{i'}(q_1)u_{j'}(q_2)\right\rangle\\ &\quad=\langle u_i'(q_1)u_j(q_2)|\mathbf{G}_{12}|u_{i'}(q_1)u_{j'}'(q_2)\rangle,\\ &\quad=u_i'(q_{1i'})\mathbf{G}(q_{1i'},q_{2j})u_{j'}'(q_{2j})\sqrt{\omega_{1i'}}\sqrt{\omega_{2j}},\end{aligned} \tag{3}$$

for a term of the kinetic energy operator, for example, and

$$\begin{aligned}&\langle u_i(q_1)u_j(q_2)|V(q_1,q_2)|u_{i'}(q_1)u_{j'}(q_2)\rangle\\ &\quad=V(q_{1i},q_{2j})\delta_{ii'}\delta jj',\end{aligned}$$

for the potential energy term. Here, $q_{\alpha i}$ and $\omega_{\alpha i}$ are the ith quadrature point and weight of the q_α coordinate, respectively.

The Hamiltonian matrix in this primitive two-dimensional basis set is transformed by the appropriate rectangular transformation matrix into one in the contracted two-dimensional basis set which is then diagonalized to give the eigenfunctions and eigenvalues.

IV. ASYMPTOTIC FORM OF WAVE FUNCTIONS

To determine the properly normalized scattering wave functions, we have to know in advance how the wave functions behave in the asymptotic region. This knowledge is obtained by solving the time independent Schrödinger equation

$$(\hat{H}-E)\Psi=0,\qquad \hat{H}(q_1,q_2)=K(q_1,q_2)+V(q_1,q_2) \tag{4}$$

as the dissociative coordinate (q_1 or q_2 depending on the arrangement channel) approaches the asymptotic region. We may expect the asymptotic form to be a product of a vibrational state in one coordinate and an outgoing or incoming wave in the other coordinate, which is consistent with the standard probability current analysis.[29]

The asymptotic Hamiltonian operator may be, when $q_1 \to \infty$, for example,

$$\hat{H}(q_1 \to \infty, q_2) = K(q_1, q_2) + V(q_1 \to \infty, q_2)$$
$$\text{or } K(q_1 \to \infty, q_2) + V(q_1 \to \infty, q_2). \tag{5}$$

Unfortunately, it is not straightforward to find such asymptotic eigenfunctions for the first form of the asymptotic $\hat{H}$, but the second form permits such asymptotic eigenfunctions. In particular, it is

$$\hat{H}(q_1 \to \infty, q_2) = \frac{-1}{2}\left(\frac{1}{\mu_{AB}} - \frac{\mu_{AC}\xi^2}{m_A^2}\right)\frac{\partial^2}{\partial q_1^2} - \frac{\nu}{m_A}\frac{\partial}{\partial q_1}\frac{\partial}{\partial q_2} + \frac{-1}{2}\frac{1}{\mu_{AC}}\frac{\partial^2}{\partial q_2^2} + U_2(q_2). \tag{6}$$

After transforming the bond coordinates to decouple the two degrees of freedom, we obtain

$$\hat{H}(q_1 \to \infty, q_2) = \frac{-1}{2M_1}\frac{\partial^2}{\partial Q_1^2} + \hat{h}_1(q_2),$$
$$\hat{h}_1(q_2) = \frac{-1}{2\mu_{AC}}\frac{\partial^2}{\partial q_2^2} + U_2(q_2), \tag{7}$$

where

$$\frac{1}{M_1} = \frac{1}{\mu_{AB}} - \frac{\mu_{AC}}{m_A^2},$$

$$Q_1 = q_1 - \frac{\nu\mu_{AC}}{m_A}q_2.$$

A similar transformation can be made for $q_2 \to \infty$. It is simple to find the flux normalized asymptotic eigenfunctions for the asymptotic Hamiltonian operator of Eq. (7), i.e.,

$$\Psi_{\text{asm}}^{\pm} = \sqrt{\frac{M_1}{k_{1n}}}\, e^{\pm ik_{1n}q_1} \cdot \tilde{\phi}_{1n}(q_2),$$
$$\tilde{\phi}_{1n}(q_2) = e^{\mp ik_{1n}\frac{\nu\mu_{AC}}{m_A}q_2}\phi_{1n}(q_2), \tag{8}$$

where the total energy $E = k_{1n}^2/2M_1 + \epsilon_{1n}$, and $\phi_{1n}(q_2)$, ϵ_{1n} is the unit normalized vibrational state and eigenvalues of the asymptotic internal Hamiltonian $\hat{h}_1(q_2)$, and k_{1n} is the corresponding wave number for that vibrational state. Similar asymptotic eigenfunctions can be found for the other arrangement channel as $q_2 \to \infty$.

The proper outgoing boundary conditions can be achieved by a linear combination of these asymptotic eigenfunctions. These conditions are imposed on a linear combination of the unnormalized FRSW's resulting in a system of linear equations to be solved for the expansion coefficients of the scattering wave functions.

V. SCATTERING WAVE FUNCTIONS AND FRANCK–CONDON INTENSITY

In this section, we detail the procedure to determine the desired scattering wave functions satisfying the outgoing scattering boundary conditions of photodissociation.

The real unnormalized FRSW which is a numerical regular eigenfunction of the total Hamiltonian in the finite range of the basis set is given by

$$\Psi_{\alpha n}(q_1, q_2) = \sum_m |m\rangle (E - \epsilon_m)^{-1} \langle m|\hat{H} - E|F_{\alpha n}\rangle + F_{\alpha n},$$
$$\alpha = 1, 2, \tag{9}$$

where $F_{1n} = f(q_1)\phi_{1n}(q_2)$, $F_{2n} = f(q_2)\phi_{2n}(q_1)$ (n is the asymptotic vibrational state quantum number), and $|m\rangle$ and ϵ_m are the discrete eigenfunction and eigenvalue, respectively. The $F_{\alpha n}$ is the energy independent auxiliary function in which $f(q_\alpha)$ is chosen conveniently as a one-dimensional linear function increasing from zero at some point near the inner boundary of the one-dimensional basis functions for q_α motion and $\phi_{\alpha n}$ is the asymptotic vibrational state of the other coordinate. The origin of $f(q_\alpha)$ must be carefully chosen such that the resulting scattering wave functions satisfy the regular boundary conditions deep inside the repulsive potential region.

The accurate scattering wave functions are linear combinations of the above unnormalized FRSW's of all open channels (N_{open}),

$$\Psi_{\alpha n}(q_1, q_2) = \sum_{\beta m}^{N_{\text{open}}} \tilde{\Psi}_{\beta m}\mathbf{C}_{\beta m, \alpha n}. \tag{10}$$

The proper expansion coefficients are determined by imposing the outgoing boundary conditions in the asymptotic region,[29]

$$\Psi_{\alpha n}(q_{\beta \to \infty}) \to \sqrt{\frac{M_\alpha}{k_{\alpha n}}}\, e^{ik_{\alpha n}q_\alpha}\tilde{\phi}_{\alpha n}\delta_{\alpha\beta} - \sum_{\gamma m}^{N_{\text{open}}} \sqrt{\frac{M_\gamma}{k_{\gamma m}}}\, e^{-ik_{\gamma m}q_\gamma}\tilde{\phi}_{\gamma m}\mathbf{S}^*_{\alpha n, \gamma m}\delta_{\beta\gamma}. \tag{11}$$

By equating Eqs. (11) and (12) at two adjacent quadrature points in the asymptotic region of each arrangement channel and projecting open vibrational states on the resulting equations, we obtain the system of linear equations which is to be solved for $\mathbf{C}$ and $\mathbf{S}$,

$$\begin{bmatrix}\mathbf{C}\\ \mathbf{S}\end{bmatrix} = \mathbf{\Omega}^{-1} \cdot \begin{bmatrix}\boldsymbol{\eta}(1)\\ \boldsymbol{\eta}(2)\end{bmatrix}, \qquad \mathbf{\Omega} = \begin{bmatrix}\mathbf{W}(1)\,\boldsymbol{\eta}(1)\\ \mathbf{W}(2)\,\boldsymbol{\eta}(2)\end{bmatrix}^*, \tag{12}$$

where

$$\mathbf{W}(i)_{\alpha n, \beta m} = \langle \phi_{\alpha n}(q_\gamma)|\tilde{\Psi}_{\beta m}(q_1, q_2)\rangle (q_{\alpha i}),$$

$$\boldsymbol{\eta}(i)_{\alpha n, \beta m} = \sqrt{\frac{M_\beta}{k_{\beta m}}}\, e^{ik_{\beta m}q_{\beta i}} \cdot \langle \phi_{\alpha n}(q_\gamma)|\, e^{-ik_{\beta m}\tilde{M}_\beta q_\gamma}\phi_{\beta m}(q_\gamma)\rangle \delta_{\alpha\beta},$$

TABLE I. System parameters.

Electron mass	$9.109\,53\times10^{-23}$ g
Hydrogen mass (H^1)	1.007 83 g/mol
Carbon mass (C^{12})	12.000 00 g/mol
Sulfur mass (S^{32})	31.972 07 g/mol
Avogadro's number	$6.022\,136\,7\times10^{23}$/mol
Hartree energy	219 474.635 4 cm^{-1}

where α, and γ are complimentary to each other (i.e., if $\alpha=1$, then $\gamma=2$, or vice versa), and $\tilde{M}_1=\nu\mu_{AC}/m_A$, $\tilde{M}_2=\nu\mu_{AB}/m_A$. Also note that the off-diagonal blocks of $\boldsymbol{\eta}$ vanish between different arrangement channels.

Note that all integrals in $\mathbf{W}(i)$ are energy independent, consequently, they need to be evaluated only once and used for other energies repeatedly. Only the small size $\boldsymbol{\eta}(i)$ matrices have to be re-evaluated at every energy.

The unit flux normalized outgoing scattering wave functions of Eq. (10) with the proper expansion coefficients of $\mathbf{C}$ matrix in Eq. (12) are used to calculate the Franck–Condon intensity $|\langle\chi_i|\Psi_f^-\rangle|^2$ at a given energy. The intensities at other energies are easily calculated since the most time consuming integral evaluations are energy independent and already done at the first energy.

If the intensities are summed for each arrangement channel, then we obtain the branching ratio, or, if summed over all final states, we obtain the quantity proportional to the total absorption cross section. Plotting the absorption cross section as a function of photon energy generates an absorption spectrum; here, we assume the transition dipole moment to be constant. If the intensity for each final state is plotted as a function of the corresponding translational energy or asymptotic internal vibrational energy, we obtain the translational or internal energy distribution at a fixed energy.

The accuracy of the calculation can be checked through the unitarity error, Δ_U,[18] of the calculated S matrix and the convergence behavior as a function of the evaluation points of Eq. (12) in addition to the usual basis set size and range.

VI. RESULTS AND ANALYSIS

In this section we present the results of several model calculations on the photodissociation of CH_3SH. All calculations are performed on the portion of the $1\ ^1A''$ potential energy surface extending from 1.6 to 5.5 a.u. in the S–H bond coordinate and 2.5 to 6.0 a.u. in the C–S bond coordinate. Two calculations were performed modeling dissociation following photoexcitation of CH_3SH in its vibrational ground state; both of these employ the $1\ ^1A''$ excited surface constructed from a two-dimensional spline fit of third order H^ν data points. One of the calculations employs a ground state $X\ ^1A'$ surface obtained from a spline fit to third order H^ν *ab initio* points; the other uses a "semiempirical" surface defined as the sum of two Morse oscillators, as described earlier. As we shall see, the most important difference between the two different ground state surfaces is the difference in the equilibrium C–S bond length, which is less for the *ab initio* spline fit surface as compared to the semiempirical surface. This difference alters the Franck–Condon overlap with the scattering wave functions on the $1\ ^1A''$ surface and profoundly affects the product branching.

TABLE II. Calculational parameters.

Basis set range	[1.6,5.5]×[2.5,6.0][a]
Basis functions	43×118→33×89[b]
1D cut energy	0.1[c]

[a]For S–H and S–C in atomic units.
[b]Primitive and contracted basis functions for S–H and S–C.
[c]Cut energy in atomic units used for one-dimensional contracted basis set determination.

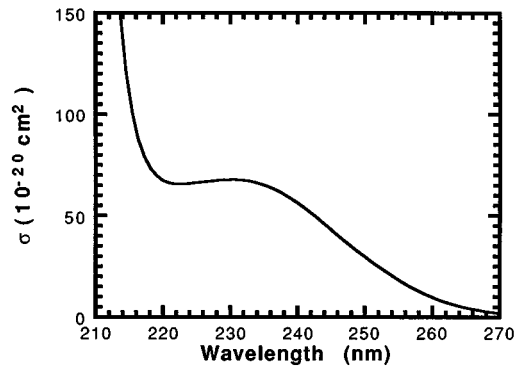

FIG. 3. The experimentally determined gas phase absorption spectrum of CH_3SH as obtained from Ref. 10. The first absorption band is shown, overlapping with the second band in the range of 210–225 nm.

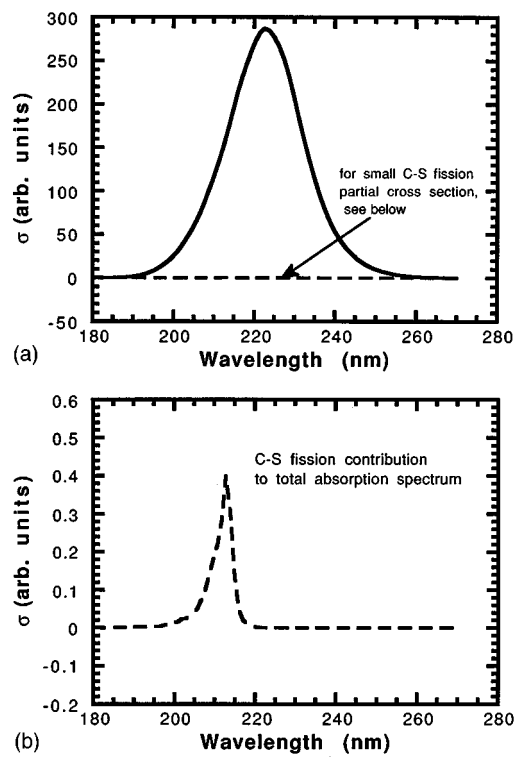

FIG. 4. The first band of the uv absorption spectrum of CH_3SH as obtained from FRSW calculations employing the *ab initio* ground state surface. The contribution to the spectrum from excitation to scattering states dissociative in the C–S bond is shown in the lower plot.

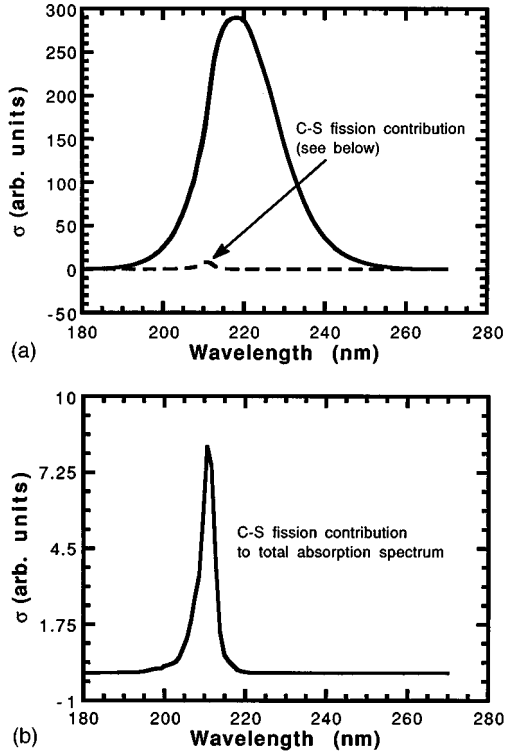

FIG. 5. The first band of the ultraviolet absorption spectrum of CH_3SH, as obtained using the semiempirical ground state surface. As in Fig. 4, the contribution to the spectrum from excitation resulting in C–S fission is shown.

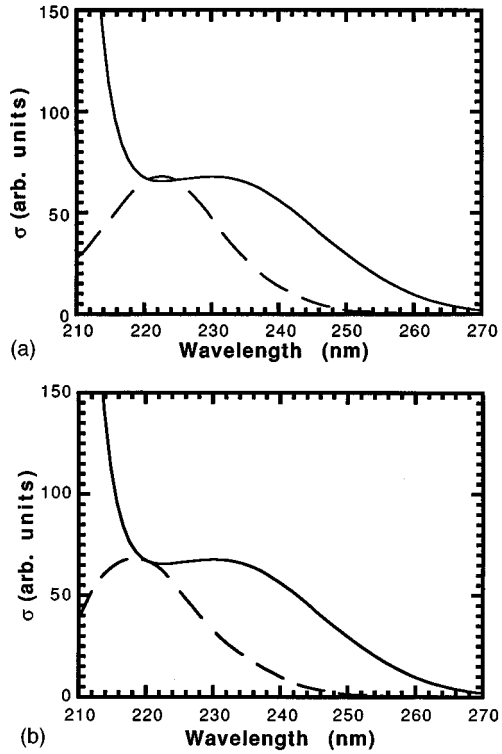

FIG. 6. A comparison of the experimental absorption spectrum of CH_3SH to spectra generated using the *ab initio* ground state surface (upper frame) and the semiempirical ground state surface (lower frame). Theoretical spectra are shown as dashed curves, the experimental spectrum is shown as a solid curve.

An additional computation uses the *ab initio* spline fit ground state surface and models the photodissociation of CH_3SH in which one quantum of excitation is placed in the C–S stretch vibrational motion prior to promotion of the molecule to the $1\ ^1A''$ surface. Tables I and II show system and calculational parameters for all FRSW calculations performed.

A. Photodissociation from the ground vibrational state

1. Absorption spectra and branching ratio

Figure 3 shows a recent experimental determination of the ultraviolet absorption spectrum of CH_3SH.[10] This spectrum may be compared to Fig. 4, the ultraviolet absorption spectrum of CH_3SH obtained from our FRSW calculation employing spline fits to the *ab initio* data for both the ground $X\ ^1A'$ and $1\ ^1A''$ states. Comparing this to experimental determinations of the absorption spectrum, Fig. 3, we find that the absorption maximum occurs at 223 nm, as compared to the experimentally found values of 227[1,1,12] and 230 nm.[10] The contribution to the total absorption spectra from excitation to scattering states which are dissociative in the carbon–sulfur bond is displayed in Fig. 4. It can readily be seen that S–H bond rupture is the primary process involved in excitation of this system; the maximum contribution to the absorption from C–S rupture occurs at 212 nm in the calculated spectrum and is found to contribute only 0.25% of the total at that wavelength.

The absorption spectrum corresponding to calculations implementing the semiempirical ground state surface is shown in Fig. 5. This spectrum reaches its maximum at 218 nm, blueshifted from the results obtained using the *ab initio*-spline ground state surface. This shift of the absorption spectrum is understandable in light of the longer C–S equilibrium bond length for the semiempirical ground state surface; superposition of the semiempirical ground state wave function on the $1\ ^1A''$ surface would show its peak located on the attractive side of the exit channel barrier to C–S bond fission, a position energetically higher than the peak of the ground state nuclear function obtained from the *ab initio*-spline ground state surface. Examining the contribution to the absorption spectrum from excitation to scattering states corresponding to C–S fission (also shown in Fig. 5) shows that the maximum contribution occurs at 211 nm and comprises 4.6% of the total at that wavelength. Hence, the shift of the ground state nuclear function toward extended C–S distances relative to the *ab initio*-spline ground state surface is seen to enhance C–S fission by more than a factor of 18.

The two calculated absorption spectra are shown superimposed on the experimental absorption spectrum in the upper and lower frames of Fig. 6. Note that the calculated absorption maximum is blueshifted relative to the experimental spectrum for the theoretical spectra resulting from both sets of surfaces. In the calculations below, when we refer to exciting the molecule at a particular wavelength, this is a wavelength within the calculated spectrum. Thus comparing the

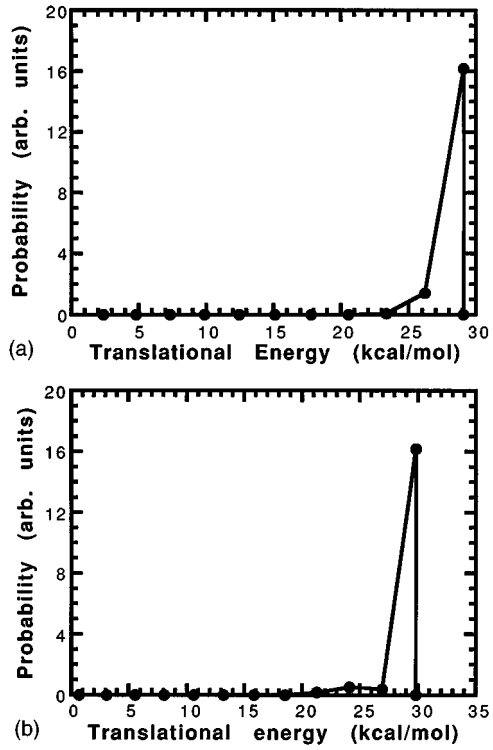

FIG. 7. Translational energy distributions for S–H bond fission calculated at 248 nm. The upper graph shows the results for the *ab initio* ground state, the lower plot shows results obtained using the semiempirical ground state surface.

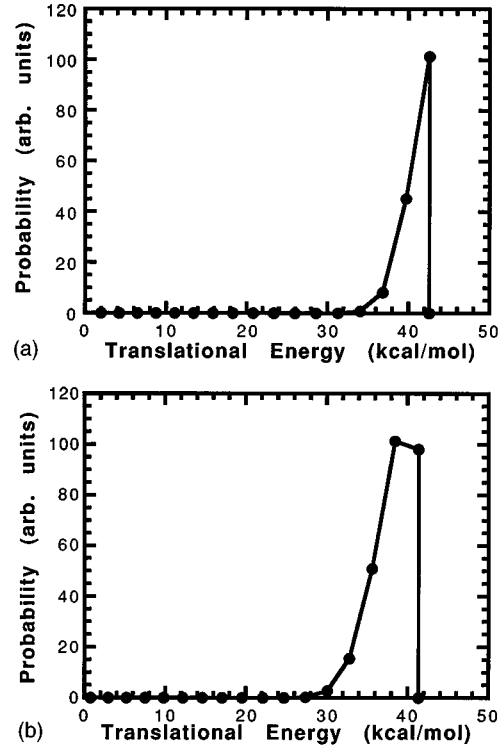

FIG. 8. Calculated translational energy distributions for S–H bond fission at 222 nm. Upper: *ab initio* ground state. Lower: semiempirical ground state.

calculation at 222 nm to the experimental results at 222 nm is not wholly accurate, as this wavelength is to the blue side of the absorption band within the experimental spectrum but near the peak in the theoretical spectra.

2. Translational and internal energy distributions of photofragments

The translational/internal energy distributions of the photofragments from S–H bond fission have been computed for comparison to experiment. The nature of the model employed is such that only the relative partitioning of energy into translation and the C–S vibrational mode can be computed; no account of energy imparted into rotations or motions of the methyl group is determined. Note that energy partitioned into vibrational modes is determined for vibrational energy levels obtained as solutions in the asymptotic regions of the calculated 1 $^1A''$ surface; e.g., the vibrational energy levels of the C–S stretching mode are found by finding solutions to the one-dimensional C–S bond motion in the asymptotic region of the S–H fission channel. These vibrational energies differ from experiment; the spacing between $\nu=0$ and $\nu=1$ vibrational levels for the C–S mode in CH_3S is found to be 1010 cm^{-1}, as opposed to the experimentally found value of 740,[30] while the spacing between $\nu=0$ and $\nu=1$ levels in the S–H mode is found to be 3009 cm^{-1}, as opposed to the experimentally found value of 2695 cm^{-1}.[31] For the translational energy distributions shown, the total available energy for partitioning into translation and vibration is determined by subtracting the potential energy minimum in the relevant asymptotic region of the 1 $^1A''$ surface from the calculation's excitation energy; for example, for S–H fission, the total available energy is found by subtracting the energy of the exciting photon from the energy minimum in the asymptotic region of the S–H bond fission channel of the 1 $^1A''$ surface.

Translational energy distributions at 248 nm may be compared to the experiments of Wittig and co-workers[8] and Butler and co-workers[7] with one caveat, described in the previous section, that the theoretical absorption spectra are shifted relative to the experimental one. Both experimental studies show that the translational energy distribution is peaked near the maximum available energy. The study of Wittig and co-workers is able to resolve a vibrational structure in the translational energy distribution from absorption at 248 nm which corresponds to a progression in the C–S stretching motion extending to $\nu=2$. The translational energy distributions at 248 nm as determined by the FRSW calculations are shown in Fig. 7. Although the calculations done with both the *ab initio*-spline ground state surface and the semiempirical surface show distributions peaked at the maximum available energy, neither calculation shows the distribution to be as broad as that found by both Butler and Wittig. In particular, neither calculation shows significant population of vibrationally excited CH_3S fragments.

The translational energy distributions computed at 222 nm, shown in Fig. 8, may be compared to those obtained by Butler and co-workers, noting the caveat above. Both the calculations performed with the *ab initio*-spline fit ground state surface and the semiempirical surface concur with experiment in that the peak is near the maximum available

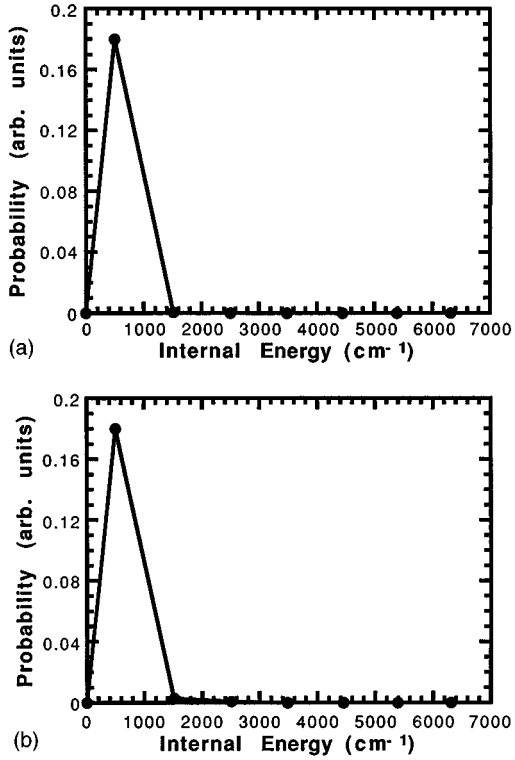

FIG. 9. Calculated internal energy distributions for S–H fission at 274 nm. Upper: *ab initio* ground state. Lower: semiempirical ground state.

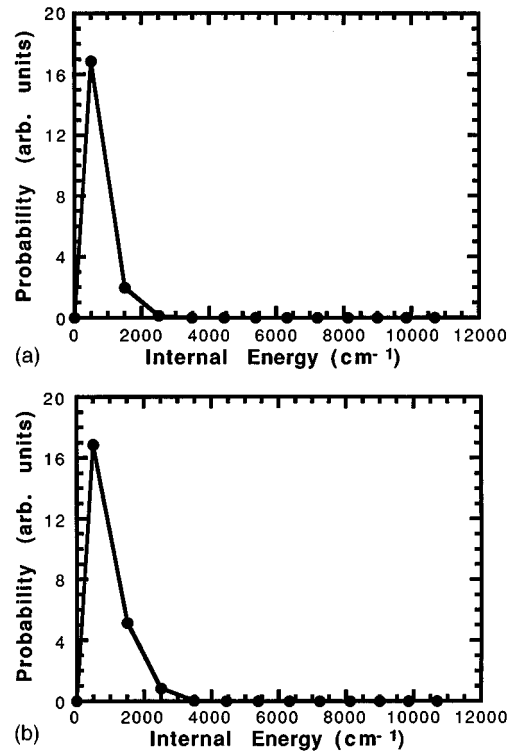

FIG. 10. Calculated internal energy distributions for S–H fission at 243 nm. Upper: *ab initio* ground state. Lower: semiempirical ground state.

energy of approximately 43 kcal/mol. The essential difference between the two computations is that the semiempirical surface gives a broader distribution with more population in the excited C–S stretch vibrational states (ν=1–4) of the CH_3S fragment than does the *ab initio* surface. This coincides more nearly with experiment than the calculation using the *ab initio* surface. One can understand why using the semiempirical ground state surface gives CH_3S fragment with more quanta in the C–S stretch very easily. Consider how the relative displacement of the ground state wave function along the C–S coordinate affects the trajectory resulting in S–H fission channel on the 1 $^1A''$ surface; the minimum of the S–H channel is located at smaller C–S internuclear distances than the minimum on either model of the ground state surface, with greater displacement relative to the semiempirical than to the *ab initio* surface. Hence, promotion of the molecule from the ground to the excited surface, followed by evolution into the S–H channel, would be expected to impart some vibrational excitation into the C–S bond. More excitation is imparted into this vibrational excitation when the calculation is performed using the semiempirical surface due to the greater displacement of the minima.

The internal energy distributions of CH_3S fragments following S–H fission which we have calculated at 247 nm (see Fig. 9) may be compared to the recent experiments of Dixon and co-workers.[9] Our calculations of potential energy surfaces do not include spin–orbit effects, and hence we do not compute the separate peaks corresponding to ground and spin–orbit CH_3S products which Dixon and co-workers are able to resolve in the internal energy distributions of CH_3S photofragments. The two computed distributions, which are not substantially different from one another, predict that CH_3S fragments will be produced almost entirely in the ν=0 state; the small population Dixon and co-workers observe in the ν=1 state is not reproduced in the calculations. Note, however, that the calculated vibrational spacing is 1010 cm^{-1} while experimentally the spacing is 740 cm^{-1}.

The computed internal energy distributions for photodissociation at 243 nm (see Fig. 10) both show population in the ν=0, 1, and 2 vibrational states of the CH_3S fragment. The calculation employing the semiempirical ground state surface determines that more CH_3S fragments should be produced with some excitation of the C–S stretch vibrational mode than does the calculation using the *ab initio*-spline fit surface. This is readily explicable in terms of the relative positioning of energy minima between the model ground and excited surfaces, as elucidated earlier. The calculations concur with Dixon's observation of increased C–S stretch excitation at this wavelength relative to 274 nm.

B. The photodissociation of vibrationally excited CH_3SH

The final calculation models the photodissociation of CH_3SH with one quantum of excitation in the C–S stretch vibrational mode (hereafter referred to as the $|01\rangle$ initial state). The calculation employs the *ab initio*-spline fit ground state surface, and will be compared to calculations of photodissociation from the vibrational ground state (the $|00\rangle$ state) which also use the *ab initio* surface. The calculated energy difference between $|00\rangle$ and $|01\rangle$ is 903 cm^{-1}; experimentally, this difference is found to be 704 cm^{-1}.[26]

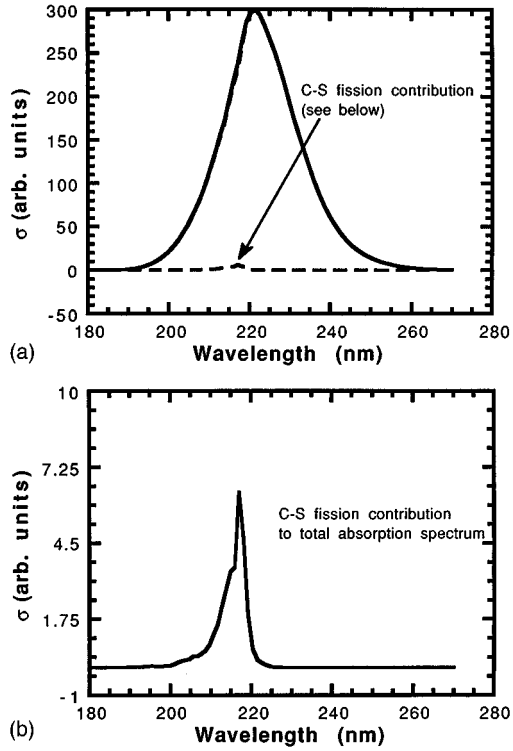

FIG. 11. The ultraviolet absorption spectrum of CH_3SH from a $|01\rangle$ initial state (top). The contribution to the spectrum from excitation resulting in C–S fission is also shown (bottom).

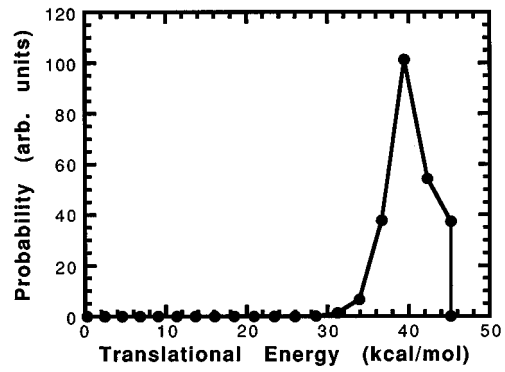

FIG. 12. Calculated translational energy distribution at 222 nm for excitation from a $|01\rangle$ initial state.

The absorption spectrum from the $|01\rangle$ initial state is shown in Fig. 11. This spectrum is slightly blueshifted relative to the spectrum of absorption from the $|00\rangle$ state. Invoking the Franck–Condon principle, one might attribute this blueshifting to preferable excitation of the vibrationally excited nuclear wave function to points on the excited potential energy surface higher than those accessed upon excitation from a ground state nuclear wave function; one would expect that points higher on the repulsive wall as well as on the exit channel barrier to C–S fission would be accessed. Photodissociation from vibrationally excited CH_3SH enhances C–S fission by a factor of 18; the C–S fission partial cross section contributes to the total absorption spectrum in the region of 210–220 nm. The enhancement of the C–S fission channel is easily understood as the result of increased degree of C–S bond motion in the ground state; the change in the ground state nuclear wave function which results from excitation of the C–S stretching mode increases the wave function's amplitude at extended C–S bond distances. This change of the Franck–Condon region improves the overlap of the ground state wave function with excited state scattering functions corresponding to C–S fission. One can think of the molecule initially promoted to the $1\ ^1A''$ surface as being positioned closer to the barrier to C–S fission, and with more vibrational motion in the C–S stretch, so that the probability of it traversing the barrier is increased.

Translational and internal energy distributions obtained from dissociation from the $|01\rangle$ ground state uniformly and predictably show more vibrational excitation of the CH_3S fragment than that which results from photoexcitation from the nuclear ground state. Figure 12 shows a representative translational energy distribution for S–H fission following excitation at 222 nm from the $|01\rangle$ state. In contrast to photodissociation from a $|00\rangle$ initial state, in which the nascent CH_3S fragments are formed primarily in the $\nu=0$ vibrational state, the $\nu=2$ state of CH_3S is formed predominantly when vibrationally excited CH_3SH is photodissociated.

VII. CONCLUSIONS

This work has simulated the dynamics of the photodissociation of CH_3SH in the first absorption band using a model in two degrees of freedom in which the dynamics is assumed to be electronically adiabatic in nature. We have shown that this model produces results which qualitatively agree with experiment in terms of absorption spectrum and product channel branching, and which predict internal energy consonant with those experimentally observed at excitation wavelengths throughout the first absorption band. This suggests that it may in fact be a good approximation to treat the dynamics as purely adiabatic in nature; that it is not necessary to consider hops from the transition state region of the $1\ ^1A''$ state to the upper, bound $2\ ^1A''$ state to adequately explain the dissociation dynamics upon excitation in the first absorption band.

One cannot, however, definitively conclude that no nonadiabatic effects play a role in the photodecomposition of CH_3SH in the first absorption band. The discrepancy between the branching ratios computed in this work and those Butler and co-workers estimate at 222 nm[7] (approximately 4% branching to C–S fission) may result from inaccuracy in the computed potential surfaces or may result from the fact that our model overlooks nonadiabatic aspects of the dynamics which enhance C–S fission. Additionally, recent calculations by Yarkony[15] indicate that conical intersections of the $1\ ^1A''$ and $2\ ^1A''$ exist which may influence the photodissociation dynamics at the blue end of the first absorption band. It is evident that calculations which include the $2\ ^1A''$ surface and it coupling to the $1\ ^1A''$ surface would provide more detail to examine the possible effects of nonadiabatic interactions on the dissociation dynamics.

ACKNOWLEDGMENTS

This work was supported by the Division of Chemical Sciences, Office of Basic Energy Sciences, Office of Energy Research, U.S. Department of Energy, under Grant Numbers DE-FG02-92ER14305 and DE-FG02-87ER13679. H.W.J. thanks Dr. C. C. Marston and Dr. K. Weide for valuable discussions and for providing the potential fitting subroutine. J. Stevens would like to thank K. F. Freed for discussions and advice.

[1] W. C. Price, J. P. Teegan, and A. D. Walsh, Proc. R. Soc., London, Ser. A **201**, 600 (1950).
[2] L. B. Clark and W. T. Simpson, J. Chem. Phys. **43**, 3666 (1965).
[3] L. Bridges and J. White, J. Phys. Chem. **77**, 295 (1973).
[4] D. F. Sheraton and F. E. Murray, Can. J. Chem. **59**, 2750 (1981).
[5] S. Nourbaksh, K. Norwood, H.-M. Yin, C.-L. Liao, and C. Y. Ng, J. Chem. Phys. **95**, 946 (1991).
[6] J. S. Keller, P. W. Kash, E. Jensen, and L. J. Butler, J. Chem. Phys. **96**, 4324 (1992).
[7] E. Jensen, J. S. Keller, G. C. G. Waschewsky, J. E. Stevens, R. L. Graham, K. F. Freed, and L. J. Butler, J. Chem. Phys. **98**, 2882 (1993).
[8] J. Segall, Y. Wen, R. Singer, M. Dulligan, and C. Wittig, J. Chem. Phys. **99**, 6600 (1993).
[9] S. H. S. Wilson, M. N. R. Ashfold, and R. N. Dixon, J. Chem. Phys. **101**, 7539 (1993).
[10] G. L. Vaghjiani, J. Chem. Phys. **99**, 5936 (1993).
[11] A. Rauk and S. Collins, J. Mol. Spectrosc. **105**, 438 (1984).
[12] B. Mouflih, C. Larrieu, and M. Chaillet, New. J. Chem. **12**, 65 (1988).
[13] B. Mouflih, C. Larrieu, and M. Chaillet, Chem. Phys. **119**, 221 (1988).
[14] J. E. Stevens, K. F. Freed, M. F. Arendt, and R. L. Graham, J. Chem. Phys. **101**, 4832 (1994).
[15] D. R. Yarkony, J. Chem. Phys. **100**, 3639 (1994).
[16] The study of Ng and co-workers (Ref. 5) at 193 nm reports the existence of a third photodissociation channel, the elimination of H_2. Other studies do not observe this channel.
[17] For examples of this phenomenon, see M. D. Person, P. W. Kash, and L. J. Butler, J. Chem. Phys. **97**, 355 (1992); P. W. Kash, G. C. G. Waschewsky, L. J. Butler, and M. M. Francl, *ibid.* **99**, 4479 (1993); P. W. Kash, G. C. G. Waschewsky, R. E. Morss, L. J. Butler, and M. M. Francl, *ibid.* **100**, 3463 (1994).
[18] H. W. Jang and J. C. Light, J. Chem. Phys. **99**, 1057 (1993).
[19] H. W. Jang, Seung E. Choi, and J. C. Light, J. Chem. Phys. **100**, 4188 (1994); S. E. Choi, M. L. Lester, H. W. Jang, and J. C. Light, *ibid.* **102**, 1981 (1995).
[20] K. F. Freed, Acc. Chem. Res. **16**, 137 (1983); Lect. Notes Chem. **52**, 1 (1989); S. Iwata and K. F. Freed, J. Chem. Phys. **65**, 1071 (1976); **66**, 1765 (1977).
[21] H. Sun, K. F. Freed, M. F. Herman, and D. L. Yeager, J. Chem. Phys. **72**, 4158 (1980); M. G. Sheppard and K. F. Freed, *ibid.* **75**, 4525 (1981); A. W. Kanzler and K. F. Freed, *ibid.* **95**, 3778 (1991); X. C. Wang and K. F. Freed, *ibid.* **91**, 3002 (1989); R. L. Graham and K. F. Freed, *ibid.* **96**, 1304 (1992); C. H. Martin, R. L. Graham, and K. F. Freed *ibid.*, **99**, 7833 (1993); J. P. Finley and K. F. Freed, *ibid.* **102**, 1306 (1995).
[22] R. Poirier, R. Kari, and I. G. Csizamadia, *Handbook of Gaussian Basis Sets, A Compendium for Molecular Orbital Calculations* (Elsevier, Amsterdam, New York, 1985).
[23] J. D. Dill and F. W. McLafferty, J. Am. Chem. Soc. **101**, 6526 (1979).
[24] T. Kojima and T. Nishikawa, J. Phys. Soc. Jpn. **12**, 680 (1957).
[25] C. C. Marston, K. Weide, R. Schinke, and H. U. Suter, J. Chem. Phys. **98**, 4718 (1993).
[26] N. P. Skerret and N. W. Thompson, Trans. Faraday Soc. **37**, 81 (1951).
[27] J. C. Light, R. M. Whitnell, T. J. Park, and S. E. Choi, in *NATO ASI Series*, edited by A. Lagana (Reidel, Kluwer, 1989), p. 187.
[28] D. E. Manolopoulos and R. E. Wyatt, Chem. Phys. Lett. **152**, 23 (1988).
[29] R. Schinke, *Photodissociation Dynamics* (Cambridge University, Cambridge, 1993).
[30] M. Suzuki, G. Inoue, and H. Akimoto, J. Chem. Phys. **81**, 5405 (1984).
[31] J. L. Dunham, Phys. Rev. **41**, 721 (1932); C. E. Moore, *Atomic Energy Levels* (Office of Standard Reference Data, National Bureau of Standards, Washington, D.C., 1971), Natl. Stand. Ref. Data Ser., Natl. Bur. Stand. Circ. No. 35.